

# Multimode vibration analysis with high-speed TV holography and a spatiotemporal 3D Fourier transform method

Cristina Trillo<sup>1\*</sup>, Ángel F. Doval<sup>1</sup>, Fernando Mendoza-Santoyo<sup>2</sup>, Carlos Pérez-López<sup>2</sup>, Manuel de la Torre-Ibarra<sup>2</sup>, J. Luis Deán<sup>1</sup>

<sup>1</sup>Departamento de Física Aplicada, E. T. S. E. Industriais, Universidade de Vigo. 36310 Vigo (Spain)

<sup>2</sup>Centro de Investigaciones en Óptica. Loma del Bosque 115, Col. Lomas del Campestre. 37150 León, Gto. (México)

\*mctrillo@uvigo.es

**Abstract:** The combination of a high-speed TV holography system and a 3D Fourier-transform data processing is proposed for the analysis of multimode vibrations in plates. The out-of-plane displacement of the object under generic vibrational excitation is resolved in time by the fast acquisition rate of a high-speed camera, and recorded in a sequence of interferograms with spatial carrier. A full-field temporal history of the multimode vibration is thus obtained. The optical phase of the interferograms is extracted and subtracted from the phase of a reference state to yield a sequence of optical phase-change maps. Each map represents the change undergone by the object between any given state and the reference state. The sequence of maps is a 3D array of data (two spatial dimensions plus time) that is processed with a 3D Fourier-transform algorithm. The individual vibration modes are separated in the 3D frequency space due to their different vibration frequencies and, to a lesser extent, to the different spatial frequencies of the mode shapes. The contribution of each individual mode (or indeed the superposition of several modes) to the dynamic behaviour of the object can then be separated by means of a bandpass filter (or filters). The final output is a sequence of complex-valued maps that contain the full-field temporal history of the selected mode (or modes) in terms of its mechanical amplitude and phase. The proof-of-principle of the technique is demonstrated with a rectangular, fully clamped, thin metal plate vibrating simultaneously in several of its natural resonant frequencies under white-noise excitation.

© 2009 Optical Society of America

**OCIS codes:** (120.6160) Speckle interferometry; (120.7280) Vibration analysis; (100.2000) Digital image processing.

---

## References

1. Á. F. Doval, "A systematic approach to TV holography," *Meas. Sci. Technol.* **11**(1), 201 (2000).
2. D. P. Towers, C. H. Buckberry, B. C. Stockley, and M. P. Jones, "Measurement of complex vibrational modes and surface form – a combined system," *Meas. Sci. Technol.* **6**(9), 1242–1249 (1995).
3. F. M. Santoyo, and G. Pedrini, Ph. Fröning, H. J. Tiziani and P. H. Kulla, "Comparison of double-pulse digital holography and HPFEM measurements," *Opt. Lasers Eng.* **32**(6), 529–536 (2000).
4. O. J. Løkberg, H. M. Pedersen, H. Valø, and G. Wang, "Measurement of higher harmonics in periodic vibrations using phase-modulated TV holography with digital image processing," *Appl. Opt.* **33**(22), 4997–5002 (1994).
5. A. R. Ganesan, P. Meinschmidt, and K. D. Hinsch, "Vibration mode separation using comparative electronic speckle pattern interferometry (ESPI)," *Opt. Commun.* **107**(1-2), 28–34 (1994).
6. J. D. R. Valera, J. D. C. Jones, O. J. Løkberg, C. H. Buckberry, and D. P. Towers, "Bi-modal vibration analysis with stroboscopic heterodyned ESPI," *Meas. Sci. Technol.* **8**(6), 648–655 (1997).
7. A. R. Ganesan, K. D. Hinsch, and P. Meinschmidt, "Transition between rationally and irrationally related vibration modes in time-average holography," *Opt. Commun.* **174**(5-6), 347–353 (2000).
8. A. J. Moore, D. P. Hand, J. S. Barton, and J. D. C. Jones, "Transient deformation measurement with electronic speckle pattern interferometry and a high-speed camera," *Appl. Opt.* **38**(7), 1159–1162 (1999).
9. C. Buckberry, M. Reeves, A. J. Moore, D. P. Hand, J. S. Barton, and J. D. C. Jones, "The application of high-speed TV-holography to time-resolved vibration measurements," *Opt. Lasers Eng.* **32**(4), 387–394 (2000).

10. W. Weaver, Jr., S. P. Timoshenko, and D. H. Young, *Vibration problems in engineering* (John Wiley & Sons, 1990), Chap. 5.
  11. H. O. Saldner, N. E. Molin, and K. A. Stetson, "Fourier transform evaluation of phase data in spatially phase-biased TV holograms," *Appl. Opt.* **35**(2), 332–336 (1996).
  12. C. Trillo, and Á. F. Doval, "Spatiotemporal Fourier transform method for the measurement of narrowband ultrasonic surface acoustic waves with TV holography," *Proc. SPIE* **6341**, 63410M–1-6 (2006).
  13. H. W. Press, B. P. Flannery, S. A. Teukolsky and W. T. Vetterling, "Fourier transform spectral methods" in *Numerical Recipes in C*, (Cambridge University Press 1988).
  14. J. L. Deán, C. Trillo, Á. F. Doval, and J. L. Fernández, "Determination of thickness and elastic constants of aluminum plates from full-field wavelength measurements of single-mode narrowband Lamb waves," *J. Acoust. Soc. Am.* **124**(3), 1477–1489 (2008).
  15. R. McCluney, *Introduction to Radiometry and Photometry* (Artech House, 1994), Chap. 8.
- 

## 1. Introduction

TV holography, also known as ESPI, is a well-established speckle interferometry technique based on the electronic recording of full-field interferograms, formed from the interference of a reference beam and the light scattered by the object to be measured [1]. Among the wide range of applications, vibration analysis of resonant modes has been carried out with a variety of illumination schemes and phase evaluation methods [2, 3]. Several authors have already addressed the problem where an excited object vibrates in several modes simultaneously. This is a realistic scenario for an object that is subjected to natural excitation under its normal operating conditions. Different approaches have been proposed to separate the vibration into its constituent resonant modes by using time-average [4, 5] or stroboscopic methods [6]. However, difficulties usually arise if more than two modes are present or if the ratio of the frequencies is an integer number, though a solution for the latter has been proposed for time-averaging [7]. The outputs are fringe patterns or one map of the amplitude and phase of the vibration obtained with a phase-stepping procedure.

TV holography is a full-field technique, so the measurement is performed simultaneously in all the field of view, without the need to scan the surface. The spatial sampling rate is then very high, but the temporal sampling rate achievable with standard cameras is rather low (usually 30 frames per second (fps) or less). With the advent of high-speed cameras, the acquisition of time-resolved measurements was possible. Naturally, they were applied to the study of transient or random vibrations [8]. Buckberry et al. [9] have reported the use of a high speed camera for the time-resolved measurement of multimode vibrations, but no attempt was made to separate the contributions of the constituent resonant modes.

In this work we present the combination of a high-speed TV holography system and a 3D Fourier-transform processing of the data for the analysis of multimode vibrations in plates. In a first stage, the out-of-plane displacement of the multimode vibration is resolved in time by the fast acquisition rate of a high-speed camera, and recorded in a sequence of interferograms. These are processed with a 2D-Fourier transform method to obtain their optical phase and a sequence of *optical phase-change maps*, that are proportional to the out-of-plane displacement undergone by the object between any given state and a reference state. In a second stage, these data are processed with a 3D Fourier transform that separates the constituent modes of the multimode vibration in the frequency space, and permits their isolation by means of bandpass filters. Contributions to the dynamic behaviour of the object due to single resonant modes or the superposition of several modes can be isolated and studied separately. The structure of the paper is as follows: first, a brief overview of resonant modes and their nomenclature is given in section 2.1. The method used to calculate the optical phase-change maps is sketched in section 2.2. Section 3 is devoted to the 3D Fourier transform processing applied to the data. Section 4 contains a detailed explanation of the experimental setup and procedure. Finally, some results obtained with a rectangular, fully clamped, thin metal plate excited with white noise are presented and discussed in section 5.

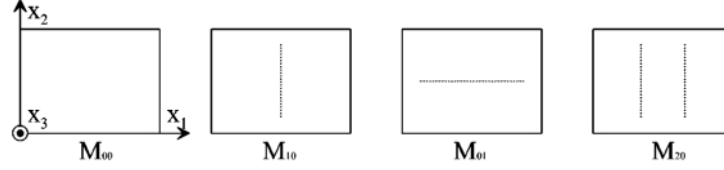


Fig. 1. Scheme of the reference system and nomenclature of some vibration modes. The dotted lines represent nodal lines.

## 2. Background

### 2.1 Vibration modes

The equation of the deflection of a simply supported rectangular plate during vibration [10] can be written as

$$u_3 = \sum_{l=0}^L \sum_{m=0}^M u_{3e,lm}(x_1, x_2, l, m) \sin\left[\frac{(l+1)\pi}{a} x_1\right] \sin\left[\frac{(m+1)\pi}{b} x_2\right] \cos(\omega_{lm} t) \quad (1)$$

with

$$\omega_{lm} = \pi^2 \sqrt{\frac{D}{\rho h} \left[ \frac{(l+1)^2}{a^2} + \frac{(m+1)^2}{b^2} \right]}, \quad D = \frac{Eh^3}{12(1-\nu^2)} \quad (2)$$

where  $u_3 = u_3(x_1, x_2, t, l, m)$  is the deflection of the plate along direction  $x_3$  (see Fig. 1),  $a$  and  $b$  are the horizontal and vertical dimensions of the plate respectively,  $E$  and  $\nu$  are the Young's modulus and Poisson's ratio,  $h$  is the plate thickness and  $\rho$  is the mass per unit volume or volumetric mass density. Each pair of integers  $(l, m)$  corresponds to a particular vibration mode, that we name according to the number of nodes (out of the edge of the plate) in the horizontal and vertical directions. For example, for  $l=0$  and  $m=0$  we have the vibration mode  $(0,0)$ , designated as  $M_{00}$  henceforth. Although our object is a fully clamped plate, its thickness is much smaller than its transversal dimensions, so the simpler model of a simply supported plate can be used to a first approximation to the problem.

### 2.2 Measurement method. Calculation of optical phase-change maps

The general expression of an interferogram with spatial carrier, recorded with single-pulse illumination, for a given instant  $t_n$  is given by [1]

$$I_n = gI_{0,n} \{1 + V_n \cos(\psi_{p,n} + \phi_{o,n} - \phi_{r,n} + 2\pi \mathbf{f}_c \cdot \mathbf{x})\} \quad (3)$$

where  $\mathbf{x} = (x_1, x_2)$  is the position on the image plane expressed in terms of the plate coordinates,  $I_n = I_n(\mathbf{x})$  is the  $n$ -th interferogram recorded at the instant  $t_n$ ,  $g = g(\lambda)$  is the spectral sensitivity of the camera at the wavelength  $\lambda$  of the laser source,  $I_{0,n} = I_{0,n}(\mathbf{x})$  is the local central value of the intensity,  $V_n = V_n(\mathbf{x})$  is the local visibility,  $\psi_{p,n} = \psi_{p,n}(\mathbf{x})$  is the random phase due to the speckle,  $\phi_{o,n} = \phi_{o,n}(\mathbf{x}, t_n)$  is the object phase related to the displacements of the object, and  $\phi_{r,n} = \phi_{r,n}(\mathbf{x}, t_n)$  is the reference phase. The term  $2\pi \mathbf{f}_c \cdot \mathbf{x}$ , with  $\mathbf{f}_c = (f_{c1}, f_{c2})$ , is the spatial carrier that allows extraction of the optical phase from the interferogram.

With the illumination and observation geometry that we have selected for our experiments, the term  $\phi_{o,n}$  is proportional to the instantaneous out-of-plane displacement field  $u_3$  at the plate surface

$$\phi_{o,n} = -\frac{4\pi}{\lambda} u_3 \quad (4)$$

Taking into account Eq. (1), this dependency can be rewritten as

$$\phi_{o,n} = -\frac{4\pi}{\lambda} \sum_{l=0}^L \sum_{m=0}^M u_{3e,lm} \sin\left[\frac{(l+1)\pi}{a} x_1\right] \sin\left[\frac{(m+1)\pi}{b} x_2\right] \cos(\omega_{lm} t_n) = \sum_{l=0}^L \sum_{m=0}^M \phi_{3e,lm} \cos(\omega_{lm} t_n) \quad (5)$$

where  $\phi_{3e,lm} = \phi_{3e,lm}(x_1, x_2, l, m)$  is the mode shape (only the factors with spatial dependence) expressed in optical terms.

An established procedure based on the spatial Fourier transform method [11] is then used to calculate the optical phase-change  $\Delta\Phi$  between two interferograms, as described by Eq. (3), one of them taken as a reference state. The result is a 2D map of the instantaneous out-of-plane displacement field between the state at the instant  $t_n$  and the reference state

$$\Delta\Phi_n = \phi_{o,n} - \phi_{o,ref} = \sum_{l=0}^L \sum_{m=0}^M [\phi_{3e,lm} \cos(\omega_{lm} t_n) - \phi_{3e,lm} \cos(\omega_{lm} t_0)] \quad (6)$$

with  $\Delta\Phi_n = \Delta\Phi_n(x_1, x_2, t_n, l, m)$ . A time sequence of these optical phase-change maps is the input for the second stage of the measurement method that we will explain in the following section.

### 3. Theory. Data processing with a spatiotemporal 3D Fourier transform

This data processing method was first devised for ultrasonic travelling waves [12] but it can be applied to any 3D array of data with spatial and/or temporal carriers. A scheme of the procedure is shown in Fig. 2. A sequence of  $N$  2D optical phase-change maps of the vibration, acquired in consecutive instants, constitute a 3D set of data that fulfil these requirements. Indeed, Eqs. (5) and (6) show that the data have a spatial carrier and, more importantly in our present case, that there is one or several temporal carriers given by the vibration frequencies  $\omega_{lm}/2\pi$  of the modes.

The discrete 3D set of experimental data of  $P \times Q \times N$  sampled points can be expressed as

$$\Delta\Phi(x_{1p}, x_{2q}, t_n, l, m) = \Delta\Phi(x_{10} + p\Delta x_1, x_{20} + q\Delta x_2, t_0 + n\Delta t, l, m) \quad (7)$$

with  $p=0 \dots P-1$ ,  $q=0 \dots Q-1$  and  $n=0, \dots, N-1$ .  $\Delta x_1$  and  $\Delta x_2$  are the spatial sampling distances in the horizontal and vertical directions respectively, and  $\Delta t$  is the temporal sampling interval. The discrete spatial and temporal sampling frequencies in  $x_1$ ,  $x_2$  and  $t$  are given by

$$f_{p'} = \frac{p'}{P\Delta x_1}, f_{q'} = \frac{q'}{Q\Delta x_2}, f_{n'} = \frac{n'}{N\Delta t} \quad (8)$$

respectively, with  $p'=-P/2, \dots, P/2$ ,  $q'=-Q/2, \dots, Q/2$  and  $n'=-N/2, \dots, N/2$ .

The 3D discrete Fourier transform of this set of data is then

$$\Delta\Phi' = DFT(\Delta\Phi) = \sum_{p=0}^{P-1} \sum_{q=0}^{Q-1} \sum_{n=0}^{N-1} \left\{ \sum_{l=1}^L \sum_{m=1}^M [\phi_{3e,lm} \cos(\omega_{lm} t_n) - \phi_{3e,lm} \cos(\omega_{lm} t_0)] \right\} \times \exp(j2\pi p p' / P) \exp(j2\pi q q' / Q) \exp(j2\pi n n' / N) \quad (9)$$

This is equivalent to calculating the sum of the 3D discrete Fourier transforms of each mode  $(l, m)$  so, in the following, we restrict the calculation to just one mode for simplicity.

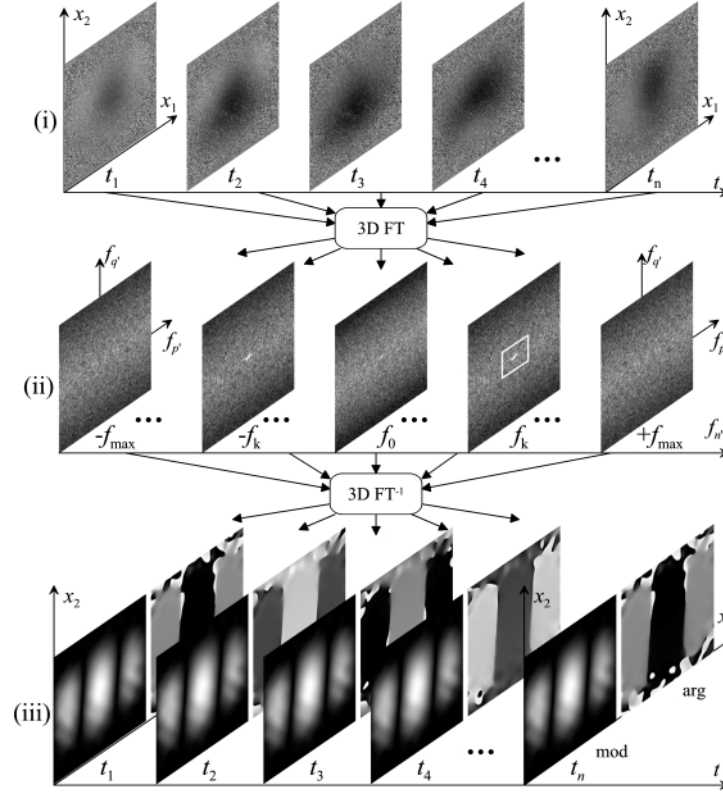


Fig. 2. Scheme of the spatiotemporal 3D Fourier transform method. (i) Sequence of optical phase-change maps of a multimode vibration. (ii) Several planes of the spatiotemporal 3D spectrum. The spectral content of one mode (with temporal frequency  $f_k$ ) of the multimode vibration is shown in planes  $\pm f_k$ . Planes with the spectral content of other modes are omitted. Planes at temporal frequencies  $f_0$  and  $f_{max}$  do not contain information. The filter used to select one of the side lobes is also shown. (iii) Mechanical amplitude and phase of the selected mode (modulus and argument of the complex data respectively).

Since  $\phi_{3e,lm}$  does not depend on time, the Fourier transform may be separated

$$\begin{aligned} \Delta\Phi'_{lm} &= \sum_{p=0}^{P-1} \sum_{q=0}^{Q-1} \phi_{3e,lm} \exp(j2\pi pp'P) \exp(j2\pi qq'Q) \sum_{n=0}^N \cos(\omega_{lm} t_n) \exp(j2\pi nn'N) \\ &\quad - \sum_{p=0}^{P-1} \sum_{q=0}^{Q-1} \phi_{3e,lm} \exp(j2\pi pp'P) \exp(j2\pi qq'Q) \sum_{n=0}^N \cos(\omega_{lm} t_0) \exp(j2\pi nn'N) \end{aligned} \quad (10)$$

and we can write

$$\begin{aligned} \Delta\Phi'_{lm} &= DFT(\phi_{3e,lm}) DFT[\cos(2\pi f_{lm} t_n)] - DFT(\phi_{3e,lm}) DFT[\cos(2\pi f_{lm} t_0)] \\ &= \frac{\phi'_{3e,lm}}{2} [\delta(n' - n'_{lm}) + \delta(n' + n'_{lm})] - \phi'_{3e,lm} \delta(n') \end{aligned} \quad (11)$$

where  $n'_{lm}$  is the frequency index of the discrete temporal frequency which is nearest to the temporal frequency  $f_{lm}$  of mode  $(l,m)$ . The spectral content of the mode is thus symmetrically shifted with respect to the zero temporal frequency, and a bandpass filter can be applied to select one of the side lobes

$$\Delta\Phi_{lm}^F = \frac{\phi'_{3e,lm}}{2} \delta(n' - n'_{lm}). \quad (12)$$

The inverse Fourier transform of the filtered data in Eq. (12) yields  $N$  complex-valued maps corresponding to the instants  $t_n$

$$A_{lm}(x_{1p}, x_{2q}, t_n, l, m) = DFT^{-1}(\Delta\Phi_{lm}^F) = \frac{1}{2} \phi_{3e,lm}(x_{1p}, x_{2q}, l, m) \exp(j2\pi f_{lm} t_n) \quad (13)$$

The modulus of this complex amplitude is proportional to the mechanical amplitude of the mode

$$\text{mod}(A_{lm}) = \sqrt{\text{Re}^2(A_{lm}) + \text{Im}^2(A_{lm})} = \frac{\phi_{3e,lm}}{2} = -\frac{2\pi}{\lambda} u_{3e,lm} \sin\left[\frac{(l+1)\pi}{a} x_{1p}\right] \sin\left[\frac{(m+1)\pi}{b} x_{2p}\right] \quad (14)$$

The argument yields the mechanical phase

$$\arg(A_{lm}) = \arctan \frac{\text{Im}(A_{lm})}{\text{Re}(A_{lm})} = 2\pi f_{lm} t_n \quad (15)$$

and the real part is proportional to the instantaneous plate deflection

$$\text{Re}(A_{lm}) = -\frac{2\pi}{\lambda} u_{3e,lm} \sin\left[\frac{(l+1)\pi}{a} x_{1p}\right] \sin\left[\frac{(m+1)\pi}{b} x_{2p}\right] \cos(2\pi f_{lm} t) \quad (16)$$

If the same process is applied to all the modes in the corresponding temporal frequencies, Eq. (13) becomes

$$A(x_{1p}, x_{2q}, t_n, l, m) = \sum_{l=0}^L \sum_{m=0}^M \frac{1}{2} \phi_{3e,lm}(x_{1p}, x_{2q}, l, m) \exp(j2\pi f_{lm} t_n) \quad (17)$$

## 4. Experimental procedure

### 4.1 Experimental setup

The TV holography system is shown in Fig. 3. It consisted of a continuous wave laser Coherent Verdi v6 ( $\lambda=532$  nm), a high-speed camera NAC Memrecam GX-1 and a speckle interferometer with sensitivity to out-of-plane displacements. The test object was a thin aluminium plate with clamped edges and dimensions 190 mm  $\times$  140 mm  $\times$  1 mm, sprayed with dry developer powder. A rectangular aperture and a lens of focal length 100 mm were used to form an image of the plate on the CMOS sensor. The pixel size of the camera was 21.7  $\mu\text{m}$   $\times$  21.7  $\mu\text{m}$ . A spatial carrier to extract the optical phase was introduced in every interferogram by tilting the reference beam slightly off axis.

Several of the lowest frequency vibration modes of the plate were simultaneously excited by means of a loudspeaker driven by an audio amplifier. The audio signal was white noise, generated with the free software *Audacity* and exported to a .wav file of duration 40 s. An ordinary mp3/wav player connected to the amplifier was used to play the file. The frequencies of the first four vibration modes were known to be approximately 320 Hz for  $M_{00}$ , 560 Hz for  $M_{10}$ , 777 Hz for  $M_{01}$  and 890 Hz for  $M_{20}$ .

### 4.2 Data acquisition and processing of optical phase-change maps

A full-field temporal history of the vibration was recorded during a time interval of 272.47 ms in  $N_{rec}=970$  interferograms with a bit depth of 12 bits per pixel. The frame rate of the camera  $f_{frame}$  is programmable in steps of one frame per second and was set to  $f_{frame}=4f_{20}=3560$  frames per second, four times the frequency of  $M_{20}$ . To freeze the vibration, the exposure time during each frame ( $T_{exp}$ ) was set to 100  $\mu\text{s}$  by the electronic shutter of the camera. The effective integration time was thus kept below 10% of the vibration period  $T_{lm}=1/f_{lm}$  for modes up to  $M_{20}$ , so the condition of pulsed illumination assumed in section 2.2 is acceptable. The

acquisition of the interferograms was manually triggered several seconds after starting the excitation, to ensure that the vibration modes had time enough to build up. Therefore, a stationary motion was assumed and an small subset  $N_{set} < N_{rec}$  of consecutive interferograms was used for the calculations. The first interferogram of the subset was taken as the reference state.

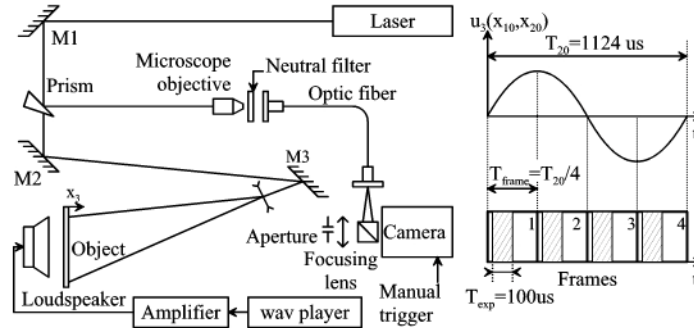


Fig. 3. Experimental setup.

To compute the Fourier transform (both 2D and 3D), a fast Fourier transform (FFT) algorithm was used [13]. It required that all the dimensions were integer powers of two, so the interferograms were padded with zeroes from the original size of 856 pixel $\times$ 848 pixel up to 1024 pixel $\times$ 1024 pixel, and a value of  $N_{set}=65$  was selected. The optical phase-change  $\Delta\Phi_n$  between the reference and the remaining interferograms was calculated as explained in section 2.2, and  $N=64$  optical phase-change maps were obtained. The value of the optical phase-change in the padded region of every map was deliberately set to zero, because it contained spurious values that affected the subsequent computation of the 3D Fourier transform. Figure 2(i) shows five of these optical phase-change maps for consecutive instants. It can be noticed that white noise was capable of exciting simultaneously several low-order modes with enough amplitude to be detected by our system.

#### 4.3 Data processing with the spatiotemporal 3D Fourier transform

A 3D Fourier transform was applied to the  $N$  maps, and a set of 64 2D complex-valued spectra were obtained. Each 2D spectrum corresponds to a set of spatial frequencies  $f_p$  and  $f_q$  and one temporal frequency  $f_n$  (see Eq. (8)). Figure 4 shows the modulus of several spectra for different values of  $n'$ . The dots replace planes corresponding to intermediate values of  $n'$  that were removed from the figure, and also indicate that the represented spectra are not equally spaced in the temporal frequency axis. In Fig. 4(i) black and white represent zero and the maximum value of the modulus respectively. Peaks near the center of the frequency spectrum appear for  $n'=0$  (DC term),  $n'=6$  ( $f_6=333,75 \text{ s}^{-1}$ ) and  $n'=14$  ( $f_{14}=778,75 \text{ s}^{-1}$ ). The latter are the spectral content of modes  $M_{00}$  and  $M_{01}$ , whose natural frequencies are very close to  $f_6$  and  $f_{14}$  respectively. Figure 4(ii) is a 3D representation that makes it easier to compare the relative height of the maxima.

The proposed 3D spatiotemporal Fourier transform method permits, in general, mode separation in space and time. For example, Deán et al. [14] separated spatially two propagating Lamb modes with the same temporal frequency taking advantage of their different wavelengths. The case herein presented is the opposite: the spatial frequencies of the excited modes are very low (see Fig. 4); therefore, the separation of different modes is generally possible only if their spectral content is distributed in different temporal frequencies. The number  $N$  of optical phase-change maps necessary to achieve the required resolution in temporal frequency depends then on the excited modes and their relative temporal frequencies. The higher the value of  $N$ , the better the resolution in the temporal frequency axis, at the cost of more RAM memory requirements and computational effort.

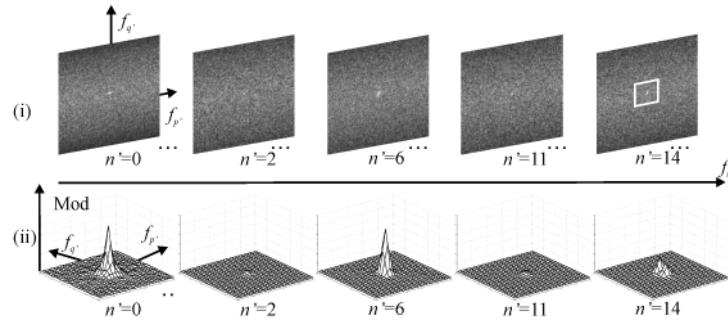


Fig. 4. (i) Modulus of several complex-valued spectra obtained after processing  $N=64$  optical phase-change maps with the spatiotemporal 3D Fourier transform. The images were equalized and only a small region of  $225 \text{ pixel} \times 225 \text{ pixel}$  around the center of the spectra is shown. Black and white represent zero and the maximum modulus respectively. A filter is shown on plane  $n'=14$ . (ii) 3D representation of a smaller region of  $25 \text{ pixel} \times 25 \text{ pixel}$ .

To assess the suitability of the chosen value  $N=64$ , the maximum modulus of the spectra was plotted versus  $n'$  in Fig. 5. Peaks for  $n'=6, 14, 16$  ( $f_{16}=890 \text{ s}^{-1}$ ) and  $26$  ( $f_{26}=1446.25 \text{ s}^{-1}$ ) are apparent. The first three match with the known frequencies of  $M_{00}$ ,  $M_{01}$  and  $M_{20}$ . The last one turned out to be  $M_{02}$ . On the contrary,  $M_{10}$  was not properly excited, since the peak at the expected frequency ( $n'=10$ ) was not discernable. The separation between peaks indicates that  $N=64$  optical phase-change maps is enough to separate the different excited modes in the frequency space.

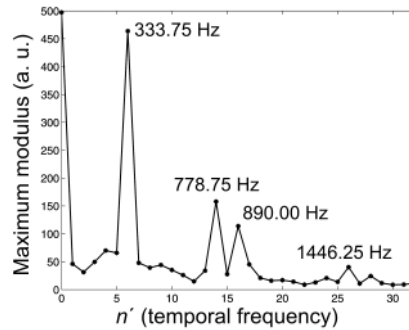


Fig. 5. Maximum modulus of the spectra versus  $n'$ . The values of temporal frequency (computed for  $\Delta t=(1/3560) \text{ s}$ ,  $N=64$ ) for the main peaks are indicated. They correspond to  $M_{00}$ ,  $M_{01}$ ,  $M_{20}$  and  $M_{02}$ .

#### 4.4 Data processing: separation of vibration modes

The resonant modes  $M_{00}$ ,  $M_{01}$ ,  $M_{20}$  and  $M_{02}$  were separated from the same set of spectra by the repeated application of the following two steps: firstly, a filtering stage; secondly, an inverse Fourier transform of the filtered data. To separate each individual mode, a single filter of rectangular shape and profile, located on the corresponding frequency plane, was used (see for example Fig. 4,  $n'=14$ ). Two different combinations of resonant modes were also separated, following the same two-step procedure. However, in this case, multiple filters located on the corresponding frequency planes were simultaneously applied. In all the cases, square filters of size  $14 \text{ pixel} \times 14 \text{ pixel}$ , symmetrical with respect to the center of the spectra, were used. As a result, six sequences of  $N=64$  complex-valued maps, corresponding to the same instants than the original sequence of optical phase-change maps, were obtained. Table 1 summarizes the information regarding this data processing and labels the obtained sequences. SM stands for “single mode” and MM for “multimode”.

**Table 1. Summary of results**

Sequence	Filters		Selected mode/s
	Number	Position	
SM1	1	$n'=6$	$M_{00}$
SM2	1	$n'=14$	$M_{01}$
SM3	1	$n'=16$	$M_{20}$
SM4	1	$n'=26$	$M_{02}$
MM1	4	$n'=6,14,16,26$	$M_{00}+M_{01}+M_{20}+M_{02}$
MM2	3	$n'=6,14,16$	$M_{00}+M_{01}+M_{20}$

The modulus of the complex data is proportional to the mechanical amplitude and the argument is equal to the vibration phase at the recording instant. The real part combines amplitude and phase and is proportional to the instantaneous deflection of the plate. An example of the modulus and argument of the complex data was shown in Fig. 2(iii). In the following figures, only a pseudo 3D representation of the real part of the complex-valued data is shown.

Regarding the data processing time, the calculation of the  $N=64$  optical phase-change maps from the 65 interferograms (section 4.2) takes about 60 s, whereas each 3D Fourier transform takes about 30 s. The whole procedure (which also involves reading from and writing data to disk) takes less than 4.5 minutes. These calculation times were obtained with a personal computer equipped with an AMD Athlon 64 3000+ processor at 1.81 GHz and 1 GB of RAM.

## 5. Results and discussion

Figures 6(a), 6(b), 6(c) and 6(d) show the instantaneous displacement of modes  $M_{00}$ ,  $M_{01}$ ,  $M_{20}$  and  $M_{02}$  respectively. The data were taken from sequences SM1, SM2, SM3 and SM4 and correspond to the same instant. The out-of-plane displacement shown in Fig. 6(e) was taken from sequence MM1, and is due to the superposition of all the modes at that same instant. Since, according to Fig. 5, these are the main resonant modes that were excited in the plate, Fig. 6(e) is the *operating deflection shape* (ODS) of the plate at that instant.

Rows (i), (ii) and (iii) in Fig. 7 show respectively the instantaneous displacement of modes  $M_{00}$ ,  $M_{01}$  and  $M_{20}$  in three consecutive instants. Row (iv), taken from sequence MM2, shows the superposition of those three modes in the same instants. This result is what we call a *filtered deflection shape* (FDS), since it is an ODS where the contribution of one of the modes present in the plate has been removed. Four multimedia files that show the 64 frames of the temporal history in these four cases are available in the online version of the journal.

All the images have a 160 mm×159 mm field of view, and were trimmed to remove the padded region. In all cases, the displacement (in nm) was obtained by applying a scale factor of  $\lambda/2\pi$  (see Eq. (16)) to the real part of the complex-valued maps.

These results show that the proposed technique can be used to analyze multimode vibrations. Individual vibration modes can be extracted from the multimode vibration and studied separately. Also, the instantaneous displacement due to any superposition of modes can be obtained by the simultaneous application of multiple filters to the data. This filtering stage also improves significantly the signal to noise ratio of the final output compared to the original optical phase-change maps.

The method does not require the synchronization of acquisition and vibration to separate the modes, neither does it impose conditions on the relative ratios of the mode frequencies. The only requirement is that the frame rate of the camera is at least twice the frequency of the highest mode of interest, to comply with the sampling theorem. In principle, no repetitions of the experiment are required to obtain a true temporal history of the vibration and, therefore, the technique is promising for the study of nonrepetitive phenomena.

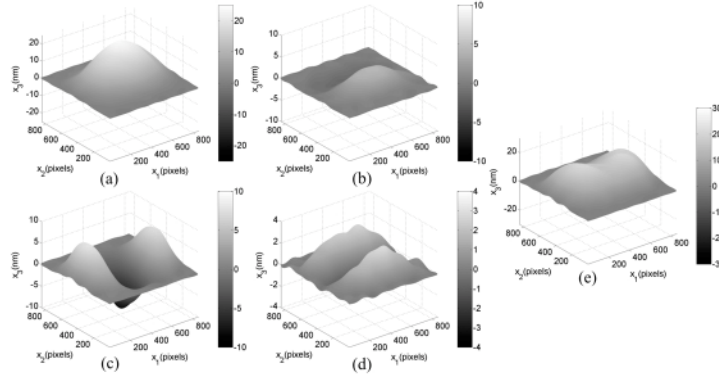


Fig. 6. Instantaneous displacement of (a) mode  $M_{00}$ , (b) mode  $M_{01}$ , (c) mode  $M_{20}$  and (d) mode  $M_{02}$ . (e) Operating deflection shape (ODS) due to modes  $M_{00}$ ,  $M_{01}$ ,  $M_{20}$  and  $M_{02}$ .

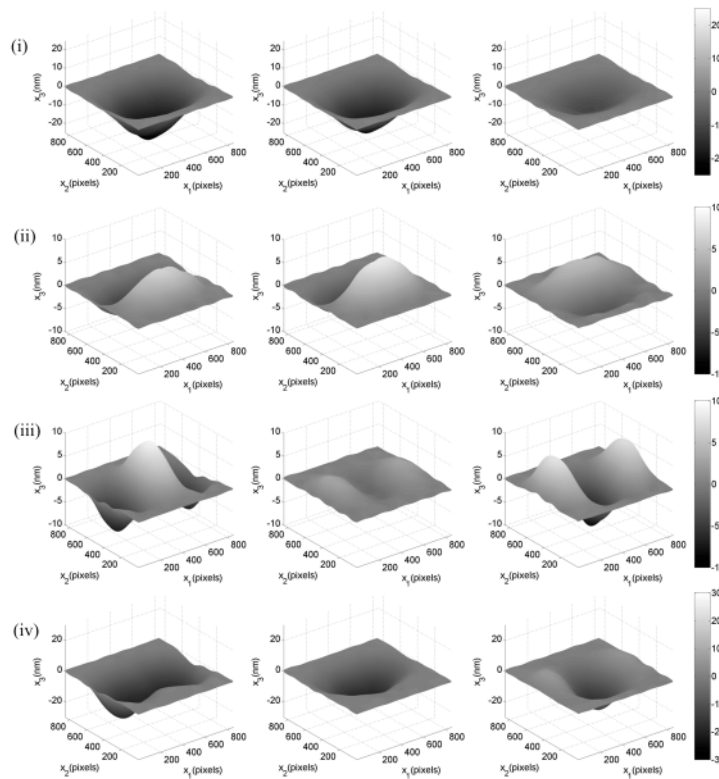


Fig. 7. Instantaneous displacement of (i) mode  $M_{00}$  ([Media 1](#)), (ii) mode  $M_{01}$  ([Media 2](#)) and (iii) mode  $M_{20}$ . ([Media 3](#)). (iv): Instantaneous displacement due to the superposition of modes  $M_{00}$ ,  $M_{01}$  and  $M_{20}$  ([Media 4](#)).

There is an intrinsic limitation on the highest-frequency mode that can be measured, due to the tradeoff between image size and frame rate: the higher the frame rate, the smaller the image size. This limitation may be overcome up to a point by making a smaller image of the object on the CMOS sensor. For example, if our current interferograms of 856 pixel  $\times$  848 pixel were fitted into an area of 512 pixel  $\times$  512 pixel, the frame rate could be increased up to 8000 fps. In any case, there would still be difficulties for combinations of very large fields of view and high order modes. However, if the phenomenon were repetitive, the herein proposed technique could still be applied to small patches of the large area that could be sequentially

inspected and subsequently stitched. Another consideration is that phase wrapping in the optical phase-change maps introduces artifacts in the spatiotemporal spectra that degrade the results. Therefore, the technique is better suited to vibrations of low amplitude (below 133 nm for our experimental conditions), that lead to non-wrapped optical phase-change maps. If vibrations of larger amplitude are to be studied, a phase unwrapping stage previous to the application of the 3D Fourier transform would be necessary.

Finally, to assess the power requirements of the system, a schematic power budget is presented. Preliminary measurements in our experimental setup showed that the illumination and reference beams carried roughly 70% and 15% of the total output power respectively. The reference beam had to be attenuated with a neutral filter. The efficiency in this stage could be improved by the use of higher quality optics that minimize losses and reduce the power diverted to the reference beam. The light impinging on the object is partly absorbed and scattered equally in all directions if the surface of the object can be considered Lambertian. Therefore, the irradiance on the image plane (i. e. the sensor) is in general a small fraction of the radiance of the object, and it is further reduced by the need to use a relatively small aperture in the optical system to resolve the speckle. The irradiance on the sensor is proportional to  $1/(f\#)^2$ , being  $f\#$  the f-number [15].  $f\#$  is also related to the speckle size  $d_s$  by  $d_s \approx 1.22 \lambda f\#$ . For a given  $\lambda$ , the minimum value of  $d_s$  that can be resolved (and therefore the maximum irradiance on the sensor) is determined by the pixel size. Assuming the  $f\#$  used in the experiments is near its optimum value, the irradiance on the sensor could be increased by tailoring the reflective properties of the object (for example, by covering it with retroreflective tape). Another feature of our system that demands high optical power is the very short exposure time  $T_{\text{exp}}$  (see Fig. 3 and section 4.1), which determines the fraction of collected light that is effectively integrated by the sensor. The selected value  $T_{\text{exp}} \approx T_{lm}/10$  lets us assume that the vibration of the object is frozen during the exposure time, being  $T_{lm}$  the temporal period of the highest mode that we want to measure confidently. In our experiments, the sampling period  $T_{\text{frame}} = 1/f_{\text{frame}}$  is set to  $T_{lm}/4$ , which is a convenient value for our phase evaluation method, as explained in Trillo et al. [12, p. 63410M-4]. The duty cycle in each frame is  $T_{\text{exp}}/T_{\text{frame}} = (0.1 T_{lm})/(0.25 T_{lm})$  and about 40% of the collected light is integrated by the sensor. Compared to an ideal optimum illumination scheme, i. e., a coherent pulsed laser capable of working at the frame rate of the camera (which would concentrate the light in the interval  $T_{\text{exp}}$ ) our system would need only 2.5 times more power to obtain the same irradiance on the sensor.

## 6. Conclusions

We have presented a novel technique for the analysis of multimode vibrations in plates. Firstly, a TV holography setup equipped with a high speed camera records a full-field temporal history of the plate deflection —i. e., its operating deflection shape, ODS— as a sequence of interferograms, from which a sequence of optical phase-change maps is calculated. A 3D array of data (two spatial dimensions and time) is thus obtained. Secondly, a 3D Fourier transform of these data separates the modes in the frequency space and allows the extraction of the individual resonant modes (or any combination of resonant modes) by means of bandpass filters. An inverse Fourier transform of the filtered data yields a sequence of complex-valued maps that contain the mechanical amplitude and phase of the selected mode or modes in the recording instants. If all the modes are considered, a smoother version of the originally ODS is obtained. The technique was successfully tested with a fully clamped aluminium plate excited with white noise and vibrating simultaneously in several of its natural resonant modes.

## Acknowledgments

This work was co-funded by the Spanish Ministerio de Ciencia e Innovación and by the European Commission (ERDF) in the context of the Plan Nacional de I+D+i (project number DPI2008-02709) and by the Dirección Xeral de Investigación, Desenvolvemento e Innovación da Xunta de Galicia in the context of the Plan Galego de IDIT (project number

INCITE08PXIB303252PR). Supplementary co-funding from Universidade de Vigo (project number I608122F64102) is also acknowledged. C. Trillo gratefully acknowledges the mobility grants received from Xunta de Galicia and Universidade de Vigo. Messrs. J. Alfredo Espinoza Pinto, Ricardo Valdivia Hernández and Jorge I. Bermúdez Rodríguez are acknowledged for their help with the excitation system.